PAPER

Synthesis and optical properties of redox-active triphenylamine-based derivatives with methoxy protecting groups†

Jung-Tsu Wu, [iD] ‡[a] Ting-Lin Hsiang‡[a] and Guey-Sheng Liou [iD] ‡*[ab]

A series of novel redox-active triphenylamine-based materials, 4,4′-bis(4,4′-dimethoxydiphenylaminyl)-4″-methoxytriphenylamine (**BDATPA**) and four related derivatives, including tris(4-methoxyphenyl)amine (**TPA**), *N,N,N′,N′*-tetrakis(4-methoxyphenyl)-1,4-phenylenediamine (**TPPA**), *N,N,N′,N′*-tetrakis(4-methoxyphenyl)-1,1′-biphenyl-4,4′-diamine (**TPB**) and tris(4-(4,4′-dimethoxyphenylaminyl)phenyl)amine (**TPAPA**), were readily prepared and their electrochemical, photoluminescence (PL) and electrochromic (EC) behaviors were investigated. Interestingly, only **TPB** exhibited high PL intensities in both solution and solid state, while the others revealed a much lower PL intensity in solution. All of these electroactive materials showed excellent electrochemical reversibility by cyclic voltammetry scanning with multi-color changes at the related oxidation states. Furthermore, UV-Vis and spectroelectrochemical measurements were also applied to evaluate and calculate the molar extinction coefficients in order to facilitate these materials as a color palette.

Introduction

To date, various energy-saving products have emerged with the growing awareness of the importance of protecting the environment. For instance, smart windows and energy storage devices[1,2] are both based on the electrochromic effect, a phenomenon of color changing that occurs when an electroactive material gains or loses one or more electrons during an electrochemical redox procedure.[3] Meanwhile, numerous luminescent materials have been studied due to their outstanding performance and tremendous potential in many applications such as organic light emitting diodes (OLEDs),[4] fluorescent biosensors,[5] solar cells,[6] and so on.

Triphenylamine (**TPA**)-based materials have been widely used for optoelectronic applications because of their advantages such as excellent electron-donating nature, easy oxidizability, light-emitting and hole-transporting capabilities.[7] Over the past twenty years, they have been developed into diverse material systems, including electropolymerized poly-**TPAs**,[8–10] conjugated polymers,[11–13] and metal complexes.[14,15] Especially, various types of high-performance polymers[16–19] (polyamides,

polyimides and epoxides) reported by our group reveal excellent electrochromic (EC) performance with interesting multi-color behavior. Furthermore, some of these triarylamine-based polymers could be applied to polymeric memory devices, while also displaying high photoluminescence (PL) capabilities in both film and fiber states.[20–26]

Recently, highly transparent to truly black electrochromic devices (ECDs) based on **TPA**-containing polyamide films were prepared as excellent shutters for next generation transparent displays.[27] However, some insufficient but crucial issues were raised when more advanced performances were requested such as the response time of the obtained polymeric ECDs. To overcome this impasse, a novel panchromatic monomeric type ECD shutter based on a structurally similar **TPA**-containing derivatives was successfully fabricated by our group recently, which could effectively enhance the EC response capability, thus greatly reducing the switching and bleaching times.[28]

In this study, we attempt to extend our effort to the design and synthesis of a series of novel **TPA**-based materials, a new compound of 4,4′-bis(4,4′-dimethoxydiphenylaminyl)-4″-methoxytriphenylamine (**BDATPA**) and other derivatives (**TPA**, **TPPA**, **TPB** and **TPAPA**) with related structures. The optical properties such as the UV-Vis absorption, PL, electrochemical stability, and EC behavior of these **TPA**-based materials were investigated and compared systematically. We expect that all of these materials can be applied not only for ECDs but also in electrofluorochromic devices (EFCDs) in the near future.

[a] *Institute of Polymer Science and Engineering, National Taiwan University, 10607, Taipei, Taiwan. E-mail: gsliou@ntu.edu.tw*

[b] *Advanced Research Center for Green Materials Science and Technology, National Taiwan University, 10607, Taipei, Taiwan*

† Electronic supplementary information (ESI) available: Experimental section, data analysis, supporting figures and tables. See DOI: 10.1039/c8tc05196h

‡ These authors equally contributed to this work.

This journal is © The Royal Society of Chemistry 2018

J. Mater. Chem. C, 2018, **6**, 13345–13351 | **13345**

Experimental

Materials

Tri-*tert*-butylphosphine, propylene carbonate (PC), toluene, *N*-methyl-2-pyrrolidone (NMP) and γ-butyrolactone (GBL) were used as received. Cesium fluoride, sodium *tert*-butoxide, sodium tetrafluoroborate and tetra-*n*-butylammonium bromide were stored in the auto dry box. Tetra-*n*-butylammonium tetrafluoroborate (TBABF$_4$) was acquired by the following process: excess saturated sodium tetrafluoroborate aqueous solution was added into a saturated tetra-*n*-butylammonium bromide aqueous solution, and the white precipitate was then filtered and recrystallized by methanol and water. **TPA, TPPA, TPB, BDATPA** and their intermediates were synthesized according to previously reported procedures.[28–30] The precursors, tris(4-nitrophenyl)amine (**TPA-3NO$_2$**) and 4,4′,4″-triaminotriphenylamine (**TPA-3NH$_2$**), of **TPAPA** can be referred to in previous literature,[31,32] and the details can be found in the ESI.† The rest of the reagents were received from a commercial source and used without further purification.

4,4′-Bis(4,4′-dimethoxydiphenylaminyl)-4″-methoxytriphenylamine (BDATPA). Tris(dibenzylideneacetone)dipalladium(0) (Pd$_2$(dba)$_3$, 55 mg, 0.060 mmol) and tri-*tert*-butylphosphine (P(*t*Bu)$_3$, 0.028 mL, 0.120 mmol) were added into a 50 mL round-bottom flask containing 20 mL anhydrous toluene in the glove box preferentially. After stirring at room temperature under nitrogen atmosphere for 10 minutes to undergo ligand exchange, 4-bromoanisole (1.51 mL, 12.0 mmol) and **TPA-2NH$_2$** (0.76 g, 2.5 mmol) were added to the flask sequentially and stirred for another 10 minutes. Sodium *tert*-butoxide (NaO*t*Bu, 1.45 g, 15 mmol) was added and then the solution was refluxed for 3 hours. After cooling to room temperature, the mixture was diluted with dichloromethane and filtered by celite. The filtrate was purified by flash column chromatography (dichloromethane/hexane: 0.5) and poured into methanol to obtain 1.67 g of pale pink powder (92% yield), mp: 245–247 °C (measured by DSC with the scan rate of 5 °C min^{-1}). FT-IR (KBr, cm^{-1}): ν = 2833, 1499, 1239, 1036, 825; ^{1}H NMR (400 MHz, C$_6$D$_6$, δ): 7.18 (d, J = 9.0 Hz, 2 H, H$_g$), 7.12 (d, J = 9.0 Hz, 12 H, H$_{b+d}$), 7.06 (d, J = 9.0 Hz, 4 H, H$_e$), 6.72 (d, J = 9.0 Hz, 10 H, H$_{c+f}$), 3.30, 3.29 (s + s, 15 H, H$_{a+h}$); ^{13}C NMR (125 MHz, C$_6$D$_6$, δ): 156.2 (C^{13}), 156.0 (C^2), 143.8 (C^9), 142.9 (C^6), 142.1 (C^{10}), 141.8 (C^5), 126.6 (C^4), 126.1 (C^{11}), 124.4 (C^8), 123.6 (C^7), 115.1 (C^{3+12}), 55.0 (C^{14+1}); Anal. calcd for C$_{47}$H$_{43}$N$_3$O$_5$: C 77.34, H 5.94, N 5.76; found: C 77.08, H 5.96, N 5.70; ESI-MS: calcd. For (C$_{47}$H$_{43}$N$_3$O$_5$)$^+$: m/z 729.32; found: m/z 729.32.

Tris(4-(4,4′-dimethoxyphenylaminyl)phenyl)amine (TPAPA). Tris(dibenzylideneacetone)dipalladium(0) (Pd$_2$(dba)$_3$, 0.280 g, 0.306 mmol) and tri-*tert*-butylphosphine (P(*t*Bu)$_3$, 0.160 mL, 0.612 mmol) were added into a 150 mL three-necked round-bottom flask containing 60 mL anhydrous toluene in the glove box preferentially. After stirring at room temperature under nitrogen atmosphere for 10 minutes to undergo ligand exchange, 4-bromoanisole (7.7 mL, 61.1 mmol) and **TPA-3NH$_2$** (2.69 g, 9.25 mmol) were added to the flask sequentially and stirred for another 10 minutes. Sodium *tert*-butoxide (NaO*t*Bu, 7.34 g, 76.4 mmol) was added

into the container and then the solution was refluxed for 3 hours. After cooling to room temperature, the mixture was diluted with dichloromethane and filtered by celite. The filtrate was purified by flash column chromatography (dichloromethane/hexane = 0.5) and poured into methanol to obtain 6.77 g of pale green powder (79%, yield), mp: 242–247 °C. FT-IR (KBr, cm^{-1}): ν = 2928, 2831, 1497, 1240, 1036, 824; ^{1}H NMR (400 MHz, DMSO-d_6, δ): 6.95 (d, J = 8.8 Hz, 12 H, H$_b$), 6.89–6.84 (m, 18 H, H$_{c+d}$), 6.75 (d, J = 8.9 Hz, 6 H, H$_e$), 3.71 (s, 18 H, H$_a$).
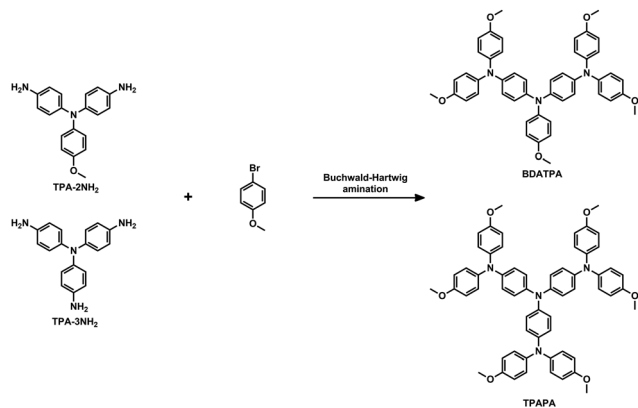
Measurement

Melting point was mainly detected by OptiMelt-Automated Melting Point System at a scan rate of 5 °C min^{-1} and DSC at a scan rate of 5 °C min^{-1}, unless otherwise stated. ^{1}H NMR and ^{13}C NMR spectra were recorded on Bruker DPX-400 NMR (400 MHz) and Bruker AVIII-500 MHz FT-NMR (125 MHz), respectively. The definition of the splitting pattern is as follows: s, singlet; d, doublet; t, triplet; q, quartet; m, multiplet. Fourier transform infrared (FT-IR) spectra were obtained from PerkinElmer Spectrum 100 Model FT-IR spectrometer. Ultraviolet-visible (UV-Vis) spectra were carried out on Agilent 8453 UV-visible Spectroscopy System. Elemental analysis (EA) was run in an elementar vario EL cube (for NCSH & O). Mass spectrometry (MS) was carried out by THERMO Q Exactive Plus. Electrochemistry was conducted with CH Instrument 611B Electrochemical Analyzer or CH Instrument 612C Electrochemical Analyzer. Cyclic voltammetry was performed at a scan rate of 50 mV s^{-1}. The parameters of the differential pulse voltammetry are listed below: scan rate of 2 mV s^{-1}, pulse amplitude of 50 mV, pulse width of 25 ms and pulse period of 0.2 s. The scan range for the spectroelectrochemical measurement is from 300 to 1100 nm. A three-electrode system combined with an optically transparent thin layer electrochemical (OTTLE) cell was used for the electrochromic investigation. An ITO coated glass or an 80 mesh platinum gauze served as the working electrode, platinum wire as an auxiliary electrode, and Ag/AgCl, 0.3 M KCl as a reference electrode.
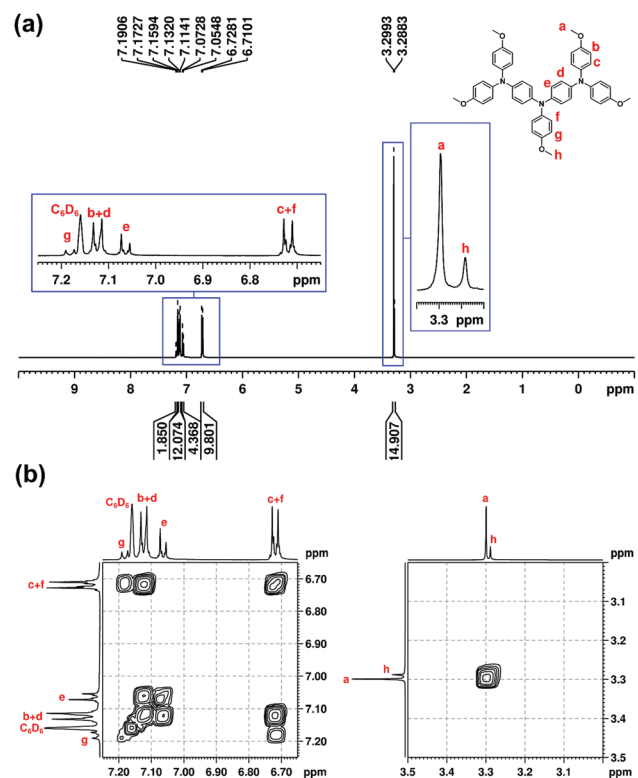
Results and discussion

Synthesis and basic characterization of the TPA-based materials

TPA, TPPA, and **TPB** were synthesized following the previous literatures using the Ullmann reaction for **TPA** and Buchwald–Hartwig amination for the others.[27–29] The preparation routes for **BDATPA** and **TPAPA** were modified from **TPPA** by obtaining the diamine or triamine intermediates first and then reacting with 4-bromoanisole (Scheme 1). The structure of the novel **BDATPA** compound was confirmed by IR (Fig. S1, ESI†) and NMR spectroscopies as shown in Fig. 1 and 2. In Fig. S1 (ESI†), the characteristic absorption peaks of –NH stretching (3000–3500 cm^{-1}) and –NH bending (∼1600 cm^{-1}) disappeared when the diamine groups were completely reacted. The ^{1}H, H–H COSY, ^{13}C and C–H HMQC NMR spectra of **BDATPA** are depicted in Fig. 1 and 2, respectively. The peak assignment for the protons and carbons

13346 | *J. Mater. Chem. C*, 2018, **6**, 13345–13351

This journal is © The Royal Society of Chemistry 2018

Scheme 1 Synthesis routes of **BDATPA** and **TPAPA**.

Fig. 1 (a) ^{1}H and (b) H−H COSY NMR spectra of **BDATPA** in C$_6$D$_6$.

Fig. 2 (a) ^{13}C and (b) C−H HSQC NMR spectra of **BDATPA** in C$_6$D$_6$.

Table 1 Optical properties of **TPA**-based materials

	TPA	TPPA	TPB	BDATPA	TPAPA
λ_{max}^{abs} [nm] (solution)	299	311	351	313	341
λ_{max}^{em} [nm] (solution)[a]	397	424	448	435	442
Φ_{PL} [%][b] (solution)	6.7	5.1	34.5	5.0	4.8
λ_{max}^{abs} [nm] (powder)	303	324	362	330	356
λ_{max}^{em} [nm] (powder)[a]	420	441	456	445	447
Φ_{PL} [%][c] (powder)		4.5	32.4		

[a] Both of λ_{max}^{em} of solution and solid state were excited at λ_{max}^{abs}. [b] The quantum yield was measured using quinine sulfate (dissolved in 1 N H$_2$SO$_4$ with a concentration of 10 μM, assuming a photoluminescence quantum efficiency of 0.546) as a standard at 25 °C. [c] PL quantum yields of molecules determined using a calibrated integrating sphere.

agreed well with the expected structure of the target compound. The ^{1}H NMR spectra of the other intermediates are also depicted in Fig. S2 and S3 (ESI†). The NMR spectrum for **TPAPA** is also added to Fig. S4 (ESI†).

Optical and electrochemical properties

The UV-Vis absorption and PL spectra of the materials were measured both in a dilute dimethyl sulfoxide (DMSO) solution (10 μM) and in the solid state, and the results are summarized in Table 1. These **TPA**-based derivatives demonstrated strong UV-Vis absorption bands with peaks at around 299–351 nm in the DMSO solution, which were assigned to the π–π* transition resulting from the resonance structures between the
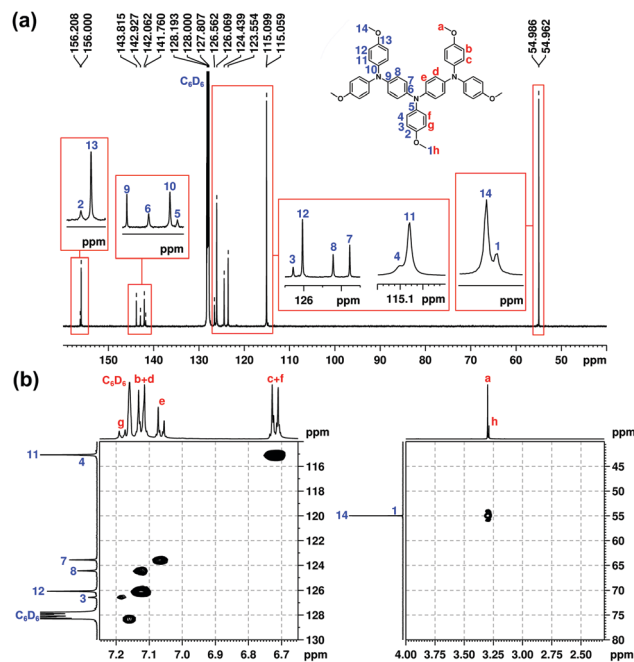
aromatic rings and the nitrogen atoms. The PL spectra for the compounds in DMSO solution displayed emitting bands with maximum peaks at around 397–448 nm within the violet-to-blue region as shown in Fig. 3. In addition, these materials in the solid state exhibited absorption peaks between 303–362 nm and PL emission peaks between 420–460 nm as summarized in Fig. 4. Interestingly, according to the PL spectra in Fig. 3 and 4, **TPB** revealed a unique PL behavior when compared with the PL intensity results of the other materials, displaying cyan emission with a maximum peak at 448 nm and a PL quantum yield of 34.5% in DMSO solution, the most intense peak was at 460 nm with a PL quantum yield of 32.4% in the solid state.
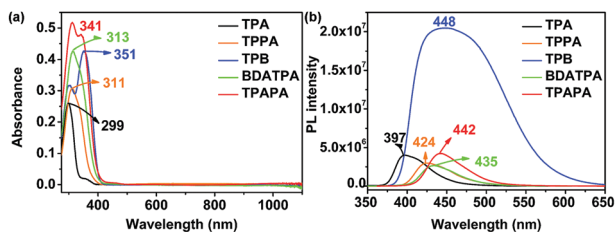
This journal is © The Royal Society of Chemistry 2018

J. Mater. Chem. C, 2018, **6**, 13345–13351 | **13347**

Fig. 3 (a) Absorption spectra and (b) PL spectra of **TPA**, **TPPA**, **TPB**, **BDATPA** and **TPAPA** in DMSO solution (solution concentration: 10 µM).
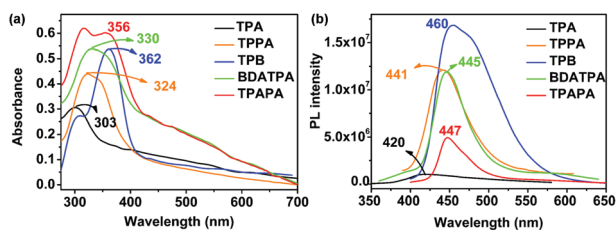

Fig. 4 (a) Absorption spectra and (b) PL spectra of **TPA**, **TPPA**, **TPB**, **BDATPA** and **TPAPA** in the solid state.

The electrochemical behavior of the as-prepared five redox-active **TPA**-based materials was investigated by cyclic voltammetry (CV) conducted with an optically transparent thin-layer electrochemical (OTTLE) cell containing solvent (propylene carbonate (PC), γ-butyrolactone (GBL), or N-methyl-2-pyrrolidone (NMP)) with 1 mM EC materials and 0.1 M tetra-n-butylammonium tetrafluoroborate (TBABF$_4$) as the supporting electrolyte under nitrogen atmosphere. These materials exhibited one to four oxidation stages corresponding to the quantity of redox nitrogen centers in their molecular structures. Fig. 5 summarizes the CV diagrams of these
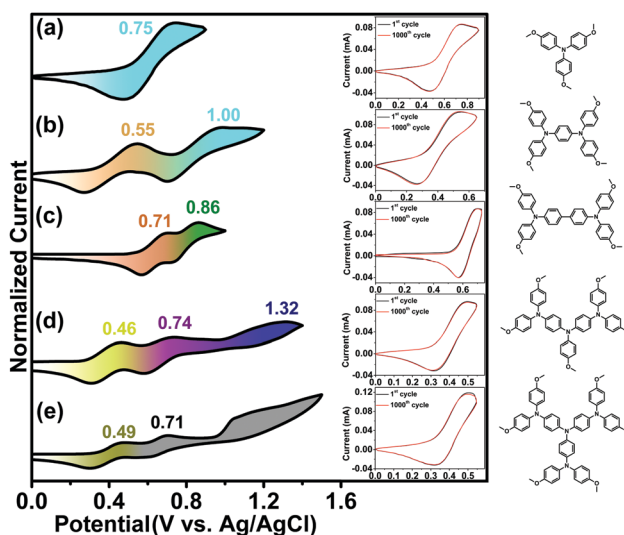

Fig. 5 Cyclic voltammetric diagrams of (a) **TPA**, (b) **TPPA**, (c) **TPB**, (d) **BDATPA**, and (e) **TPAPA** at the scan rate of 10 mV s^{-1}. Inset: Electrochemical stability measurements at the scan rate of 50 mV s^{-1} for the corresponding materials; 10^{-3} M **TPA**, **TPPA** and **TPB** were dissolved in 0.1 M TBABF$_4$/PC; 10^{-3} M **BDATPA** was dissolved in 0.1 M TBABF$_4$/GBL; 10^{-3} M **TPAPA** was dissolved in 0.1 M TBABF$_4$/NMP.

five kinds of anodic EC materials. **TPA** shown in Fig. 5a exhibited only one oxidation peak at 0.75 V, **TPPA** revealed two oxidation stages with peaks at 0.55 and 1.00 V in Fig. 5b, respectively, and **TPB** also displayed two oxidation stages, with peaks at 0.71 and 0.86 V as shown in Fig. 5c. **BDATPA** depicted in Fig. 5d displayed three oxidation redox peaks at 0.46, 0.74 and 1.32 V, respectively. Furthermore, **TPAPA** had only two clear oxidation peaks at 0.49 and 0.71 V in Fig. 5e, while Fig. S5 (ESI†) confirms that there should be four oxidation stages at 0.42, 0.69, 1.09 and 1.21 V, using differential pulse voltammetry (DPV) measurement. The introduction of para-methoxy groups into the TPA units can effectively prevent the intermolecular coupling reaction for the formation of dimers during the oxidation procedure, as reported in our previous literatures.[20] CV measurements could also be used to evidence the excellent electrochemical stability of the series of **TPA**-based derivatives between their neutral and first oxidation states for 1000 cycles, respectively, and the results shown in the insets of Fig. 5 clearly confirm the excellent redox stability of all the materials in this study.

Spectroelectrochemistry

Spectroelectrochemical measurements were employed for validating the optical behavior of the series of EC materials. Preliminary investigation of the electrochromism of five compounds was carried out by an OTTLE coupled with UV-Vis spectroscopy and the scanning conditions were replicated for the CV measurements. The results are summarized in Fig. 6 and their
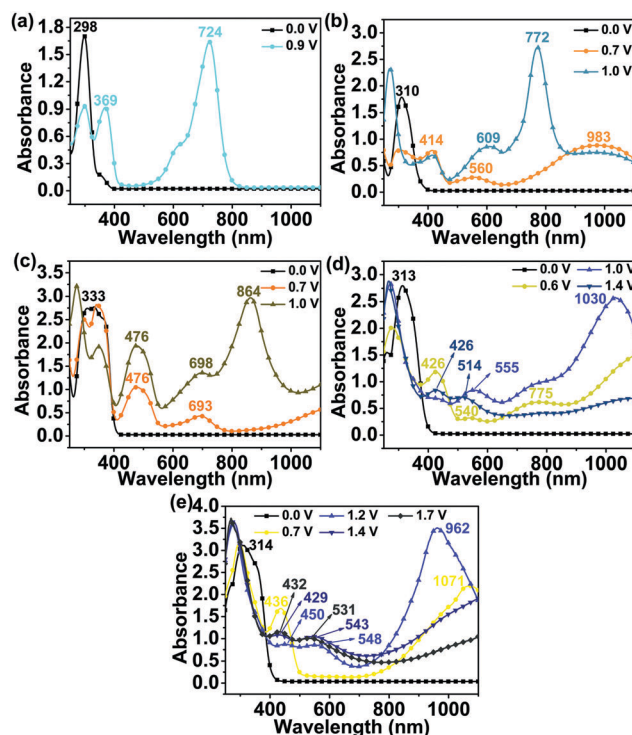

Fig. 6 Spectroelectrochemical measurements and EC behaviors of (a) **TPA**, (b) **TPPA**, (c) **TPB**, (d) **BDATPA**, and (e) **TPAPA** at applied potentials of the related oxidation stages. 10^{-3} M of **TPA**, **TPPA** and **TPB** were dissolved in 0.1 M TBABF$_4$/PC; 10^{-3} M of **BDATPA** was dissolved in 0.1 M TBABF$_4$/GBL; 10^{-3} M of **TPAPA** was dissolved in 0.1 M TBABF$_4$/NMP.
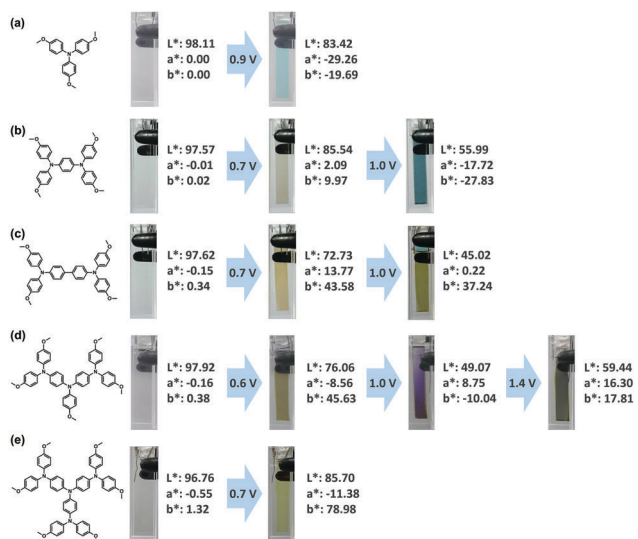
Fig. 7 Chemical structures, the corresponding electrochromism, and *L**a*b* values of (a) **TPA**, (b) **TPPA**, (c) **TPB**, (d) **BDATPA**, and (e) **TPAPA** at different oxidation states. 10^{-3} M of **TPA**, **TPPA** and **TPB** were dissolved in 0.1 M TBABF$_4$/PC, respectively; 10^{-3} M of **BDATPA** was dissolved in 0.1 M TBABF$_4$/GBL; 10^{-3} M of **TPAPA** was dissolved in 0.1 M TBABF$_4$/NMP.

corresponding color changes are depicted in Fig. 7. First, the spectroelectrochemical measurement for **TPA** is shown in Fig. 6a and the characteristic peaks appear at 369 and 724 nm corresponding to the first oxidation state, which also agrees with the previous study.[33] The optical changes of **TPPA** at different oxidation states shown in Fig. 6b reveal that the characteristic absorption peak of the neutral **TPPA** at 310 nm diminished gradually with the formation of the radical cation of **TPPA** during the first oxidation stage (0.0–0.7 V), while three new peaks at 414, 560 and 983 nm appeared simultaneously. The absorption peak in the near-IR region can be ascribed to intervalence charge transfer (IV-CT) excitation associated with the electron transfer between active neutral nitrogen and cation radial nitrogen atoms within the *p*-phenylenediamine moiety of **TPPA**, which is also consistent with the phenomenon classified by Robin and Day.[34] When higher voltages (0.8–1.0 V) were applied to achieve the second oxidation state, the peaks belonging to the first oxidation state decreased and two new peaks at 609 and 772 nm appeared, generating a blue color. Then, the characteristic absorption peak at 333 nm for the neutral form of **TPB** could be observed, which verifies the redshift caused by the more conjugated biphenyl moiety relative to the **TPPA** unit. Afterwards, three new peaks appeared during the first oxidation process, two in the visible light region (476 and 693 nm) and one in the near-IR region as shown in Fig. 6c. The IV-CT excitation of **TPB** observed at longer wavelengths of 1100 nm implies that the electronic coupling interaction between the active neutral nitrogen and the radical nitrogen cations, within the benzidine moiety of **TPB**, is weaker than the one of **TPPA** mentioned above. Then, a new intense absorption band with a peak at 864 nm appeared, and the characteristic peaks for the first oxidation state at 476 and 693 nm also increased during the second oxidation process. Fig. 6d represents the optical absorption change of **BDATPA**;

the intensity of the characteristic absorption of **BDATPA** with a peak at 313 nm decreased during the first oxidation process, while three new absorption peaks at 426, 540, 775 nm, and one broad absorption band in the near-IR region were observed. In the second stage of the oxidation process, the intensity of the peak at 426 nm weakened while the characteristic peak at 540 nm strengthened with a slight red shift, and the IV-CT band with a peak at 1030 nm was greatly enhanced. For the **TPAPA** compound, the spectral differences at varied potentials that relate to the distinctive oxidation stages are presented in Fig. 6e. The characteristic peaks at 436 and 1071 nm are generated during the first oxidation process. Then, the peak at 436 nm decreased with a slight red-shift, while the intensity of the IV-CT band increased significantly, accompanied by a slight blue-shift in the second oxidation stage. Moreover, the absorption peaks at 450 and 553 nm revealed no significant difference for the preceding third and fourth oxidation states, while the intensity of the IV-CT band subsequently decreased accompanied by a red-shift.

Furthermore, the color changes for these **TPA**-based EC materials at different oxidation stages were identified and evaluated by CIELAB data and are summarized in Fig. 7. For **TPA**, the color changed from colorless (*L**: 98.11, *a**: 0.00, *b**: 0.00) to cyan (*L**: 83.42, *a**: −29.26, *b**: −19.69); the colors that could be produced for **TPPA** ranged from colorless (*L**: 97.57, *a**: −0.01, *b**: 0.02) to light green (*L**: 80.54, *a**: 2.09, *b**: 9.97) and then intense cyan (*L**: 55.99, *a**: −17.72, *b**: −27.83). **TPB** could also bring out multi-color changes from colorless (*L**: 97.62, *a**: −0.15, *b**: 0.34) to light orange (*L**: 72.73, *a**: 13.77, *b**: 43.58), and then atrovirens (*L**: 45.02, *a**: 0.22, *b**: 37.24). For the novel **BDATPA**, it could give rise to polyelectrochromism from colorless (*L**: 97.92, *a**: −0.16, *b**: 0.38) to yellow green (*L**: 76.06, *a**: −8.56, *b**: 45.63), purple (*L**: 49.07, *a**: 8.75, *b**: −10.04), and then grey-green (*L**: 59.44, *a**: 16.30, *b**: 17.81). In the case of **TPAPA**, the color changed from colorless (*L**: 96.76, *a**: −0.55, *b**: 1.32) to yellow (*L**: 85.70, *a**: −11.38, *b**: 78.98), while the rest of the oxidation states exhibited no significant color change.

Furthermore, in order to predict the color-merging effects of these EC materials, accurate characterization of the extinction coefficients, so called absorption coefficient, would be crucial and inevitable. Thus, the molar extinction coefficients (ε, M^{-1} cm^{-1}) of these **TPA**-based derivatives at the first oxidation state was also evaluated in this study following the Beer–Lambert law ($A = \varepsilon bc$), and the results are summarized in Fig. 8. As described in Fig. 8a, the absorbance was obtained from spectroelectrochemical measurements with a concentration of 10^{-3} M and light path length of 10^{-1} cm. According to Fig. 8b, the extinction coefficient of these redox-active materials in the neutral form revealed some regularity. When the structure changed from **TPA** to **TPPA**, the absorption band in the UV region became broader, and the peak also enhanced with a red shift from 298 to 310 nm. Comparing the three structurally related **TPA**-based materials, **TPPA**, **BDATPA** and **TPAPA** with different number of multi-arylamine moieties, the peak wavelengths for their maximum absorption displayed no significant difference (310–314 nm) but exhibited greatly enhanced absorbance (1.8–3.2), molar extinction coefficients (1.8–3.2 × 10^5 M^{-1} cm^{-1}), and enlarged

This journal is © The Royal Society of Chemistry 2018

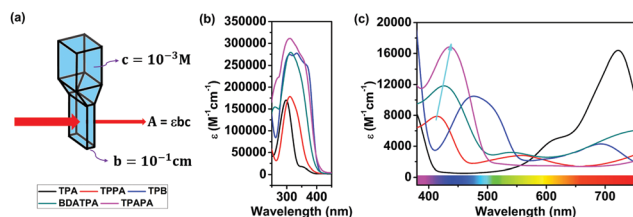*J. Mater. Chem. C*, 2018, **6**, 13345–13351 | **13349**

Fig. 8 (a) Schematic measurement of extinction coefficient, (b) extinction coefficients for these materials at their neutral states and (c) extinction coefficients for these materials at their first oxidation states. 10^{-3} M of **TPA**, **TPPA** and **TPB** were dissolved in 0.1 M TBABF$_4$/PC; 10^{-3} M of **BDATPA** was dissolved in 0.1 M TBABF$_4$/GBL; 10^{-3} M of **TPAPA** was dissolved in 0.1 M TBABF$_4$/NMP.

full width at half maximum (FWHM) corresponding to the number of arylamines within the structure of these materials. Furthermore, **TPB** gave rise to moderately higher absorbance and molar extinction coefficient values with significant red shift and enlarged FWHM when compared with those of **TPPA**, owing to the higher conjugation length of benzidine moiety. Meanwhile, the values for the molar extinction coefficient were also in good agreement with the number of arylamine units. Subsequently, the electro-optical behavior for each EC materials at their first oxidation states was investigated. The values for the absorbance, molar extinction coefficient, and the wavelength of the peak of maximum absorption for these EC materials in visible region demonstrated a similar trend as the ones at the neutral states, and the results are depicted in Fig. 8c. **TPPA**, **BDATPA** and **TPAPA** displayed their main absorption bands with the peaks ranging from 415 to 440 nm, while the main absorption peak wavelength for **TPB** appeared at around 480 nm, which could also be verified in Fig. 6.

Conclusions

A series of redox-active **TPA**-based EC materials, a novel **BDATPA** and other four structurally related derivatives were successfully prepared *via* the Ullmann reaction and Buchwald–Hartwig amination. Incorporation of the electron-donating methoxy groups into the **TPA**-based materials at the *para* position of the phenyl ring can effectively prevent coupling reactions in their oxidized states, thus the electrochemical stability of the obtained materials was greatly enhanced. In addition, **TPB** demonstrates an interesting and unique optical behavior both in solution and in solid state with high light-emission and PL quantum yields. By merging and coordinating the molar extinction coefficient data of these obtained redox-active **TPA**-based materials, the colors of different EC derivatives can be easily tuned and predicted. Thus, the application potential of fabricated ECDs can be greatly enhanced according to the resulting outcomes of our present study.

Conflicts of interest

There are no conflicts to declare.

Acknowledgements

Notes and references

1 A. Azens and C. Granqvist, *J. Solid State Electrochem.*, 2003, **7**, 64.
2 P. Yang, P. Sun and W. Mai, *Mater. Today*, 2016, **19**, 394.
3 R. J. Mortimer, *Chem. Soc. Rev.*, 1997, **26**, 147.
4 E. Morales-Narváez, L. Baptista-Pires, A. Zamora-Gálvez and A. Merkoçi, *Adv. Mater.*, 2017, **29**, 1604905.
5 T. Liu, L. Zhu, C. Zhong, G. Xie, S. Gong, J. Fang, D. Ma and C. Yang, *Adv. Funct. Mater.*, 2017, **27**, 1606384.
6 A. Labrunie, J. Gorenflot, M. Babics, O. Aleveque, S. Dabos-Seignon, A. H. Balawi, Z. P. Kan, M. Wohlfahrt, E. Levillain, P. Hudhomme, P. M. Beaujuge, F. Laquai, C. Cabanetos and P. Blanchard, *Chem. Mater.*, 2018, **30**, 3474.
7 M. Thelakkat, *Macromol. Mater. Eng.*, 2002, **287**, 442.
8 S. Cai, H. Wen, S. Wang, H. Niu, C. Wang, X. Jiang, X. Bai and W. Wang, *Electrochim. Acta*, 2017, **228**, 332.
9 P. Zhou, Z. Wan, Y. Liu, C. Jia, X. Weng, J. Xie and L. Deng, *Electrochim. Acta*, 2016, **190**, 1015.
10 S. H. Hsiao and S. W. Lin, *J. Mater. Chem. C*, 2016, **4**, 1271.
11 S. Mi, J. C. Wu, J. Liu, J. M. Zheng and C. Y. Xu, *Org. Electron.*, 2015, **23**, 116.
12 P. I. Wang, W. R. Shie, J. C. Jiang, L. J. Li and D. J. Liaw, *Polym. Chem.*, 2016, **7**, 1505.
13 C. Yang, W. Cai, X. Zhang, L. Gao, Q. Lu, Y. Chen, Z. Zhang, P. Zhao, H. Niu and W. Wang, *Dyes Pigm.*, 2019, **160**, 99.
14 J. H. Tang, Y. Q. He, J. Y. Shao, Z. L. Gong and Y. W. Zhong, *Sci. Rep.*, 2016, **6**, 35253.
15 C. B. Fan, C. Q. Ye, X. M. Wang, Z. G. Chen, Y. Y. Zhou, Z. Q. Liang and X. T. Tao, *Macromolecules*, 2015, **48**, 6465.
16 H. J. Yen, H. Y. Lin and G. S. Liou, *Chem. Mater.*, 2011, **23**, 1874.
17 H. J. Yen, C. J. Chen and G. S. Liou, *Adv. Funct. Mater.*, 2013, **23**, 5307.
18 Y. W. Chuang, H. J. Yen, J. H. Wu and G. S. Liou, *ACS Appl. Mater. Interfaces*, 2014, **6**, 3594.
19 H. J. Yen and G. S. Liou, *Polym. Chem.*, 2018, **9**, 3001.
20 J. H. Wu and G. S. Liou, *ACS Appl. Mater. Interfaces*, 2015, **7**, 15988.
21 H. J. Yen, J. H. Wu, W. C. Wang and G. S. Liou, *Polym. J.*, 2016, **48**, 117.
22 S. W. Cheng, T. Han, T. Y. Huang, Y. H. Chang Chien, C. L. Liu, B. Z. Tang and G. S. Liou, *ACS Appl. Mater. Interfaces*, 2018, **10**, 18281.
23 H. J. Yen, C. J. Chen and G. S. Liou, *Chem. Commun.*, 2013, **49**, 630.
24 H. J. Yen, J. H. Wu, W. C. Wang and G. S. Liou, *Adv. Opt. Mater.*, 2013, **1**, 668.

13350 | *J. Mater. Chem. C*, 2018, **6**, 13345–13351

This journal is © The Royal Society of Chemistry 2018

25 J. H. Wu and G. S. Liou, *Adv. Funct. Mater.*, 2014, **24**, 6422.

26 S. W. Cheng, T. Han, T. Y. Huang, B. Z. Tang and G. S. Liou, *Polym. Chem.*, 2018, **9**, 4364.

27 H. S. Liu, B. C. Pan, D. C. Huang, Y. R. Kung, C. M. Leu and G. S. Liou, *NPG Asia Mater.*, 2017, **9**, e388.

28 J. T. Wu and G. S. Liou, *Chem. Commun.*, 2018, **54**, 2619.

29 L. L. Hill, L. R. Moore, R. C. Huang, R. Craciun, A. J. Vincent, D. A. Dixon, J. Chou, C. J. Woltermann and K. H. Shaughnessy, *J. Org. Chem.*, 2006, **71**, 5117.

30 B. A. Kamino, B. Mills, C. Reali, M. J. Gretton, M. A. Brook and T. P. Bender, *J. Org. Chem.*, 2012, **77**, 1663.

31 J. H. Gorvin, *J. Chem. Soc., Perkin Trans. 1*, 1988, 1331.

32 S. C. Sun, Q. H. Shu, P. C. Lin, Y. Y. Li, S. H. Jin, X. Chen and D. Q. Wang, *RSC Adv.*, 2016, **6**, 93826.

33 D. C. Huang, J. T. Wu, Y. Z. Fan and G. S. Liou, *J. Mater. Chem. C*, 2017, **5**, 9370.

34 M. B. Robin and P. Day, *Adv. Inorg. Chem. Radiochem.*, 1968, **10**, 247.